Stimulated rotational Raman scattering by a polarization-modulated femtosecond pulse

Yuichiro Kida,[1] Shin-ichi Zaitsu,[1] and Totaro Imasaka[1,2]

[1]*Department of Applied Chemistry, Graduate School of Engineering, Kyushu University, 744, Motooka, Nishi-ku, Fukuoka 819-0395,
Japan*

[2]*Center for Future Chemistry, Kyushu University, 744, Motooka, Nishi-ku, Fukuoka 819-0395, Japan*

Transient stimulated rotational Raman scattering induced by a polarization-modulated femtosecond pulse whose polarization varies with time is reported. The peak intensity of the polarization-modulated pulse produced in this study is low compared to that of a pulse without polarization variation, and this leads to the low efficiency of self-phase-modulation and thus the high efficiency of stimulated Raman scattering compared to the case of a pump pulse without polarization modulation. The scattering process is unique in terms of the high peak ratio of the anti-Stokes to Stokes emissions compared to the ratio in the case of the scattering induced by linearly, circularly, and elliptically polarized pump pulses. Under optimum conditions, the ratio approaches 1, which is not realized in the general case of stimulated rotational Raman scattering.

I. INTRODUCTION

A laser system producing pulses with high intensities and extremely short widths has been utilized in studies of nonlinear optical phenomena. One such phenomenon is stimulated Raman scattering (SRS) [1,2], which modulates the frequency of an optical pulse to a different frequency depending on the vibrational or rotational periods of the Raman medium. Numerous emission lines can be generated by SRS in the spectral range from the ultraviolet (uv) to near-infrared regions by focusing nanosecond [3], picosecond [4], and femtosecond [5,6] pulses into pressurized hydrogen gas. If a femtosecond pulse is focused into hydrogen gas, SRS is caused in a highly transient regime since the pulse width is much shorter than the dephasing time (picosecond time scale) of coherent rotations or vibrations of hydrogen molecules. Since the scattering efficiency of transient SRS (TSRS) depends on the energy rather than the intensity (and thus the pulse width) of a pump pulse [7], it is expected that the use of a high-energy pulse will result in an increase in the generation efficiency of TSRS. This is, however, not always true, especially in the case of an extremely short pump pulse, whose width is several hundreds of femtoseconds or less, since it also induces another nonlinear optical phenomenon such as self-phase modulation (SPM). The generation of SPM competes with TSRS and substantially suppresses the Raman emission efficiency, which becomes a serious problem especially in the case of a near-ir pump pulse and a Raman medium with low density [6].

Several approaches have been reported to solve this problem. One such solution relates to the use of a seed beam whose frequency corresponds to that of the Stokes emission, which is generated by use of an optical parametric amplifier (OPA) [8]. In this case, vibrational Raman emissions were generated in the spectral range from the near-ir to uv region using slightly stretched pulses. The use of a femtosecond pulse reshaped in a novel gas is another idea. Here, a sharp spikelike structure formed in the pulse, which is shorter than the period of molecular rotation, excites coherent molecular motions impulsively and generates a strong Stokes emission

[9]. The pump-probe technique [10,11] can also be used to improve the Raman emission efficiency. In this regime, coherent rotations (vibrations) of Raman active molecules are excited impulsively [10,12] or transiently [11,13] using a high-energy pulse (pump pulse), and then a relatively low-energy pulse (probe pulse) is passed through the excited medium to generate Raman emissions. Since the efficiency of the energy conversion is independent of the intensity of the probe pulse, Raman emissions can be generated even when the energy of the probe pulse is extremely low. The generation of SPM, therefore, can be removed by keeping the energy of the probe pulse below the threshold of the phase modulation. Though the approaches shown above are useful, they require a relatively complicated experimental setup and do not increase the threshold energy for the generation of SPM.

In this paper, transient stimulated rotational Raman scattering (TSRRS) induced by a femtosecond pulse whose polarization varies with time (hereafter denoted as a polarization-modulated pulse) is investigated. A polarization-modulated pulse prepared in this study has a low peak intensity compared to a pulse without polarization modulation, and this leads to the low efficiency of SPM which reduces the efficiency of the Raman emission. The process of TSRRS in this regime is unique in terms of the high peak ratio of the anti-Stokes emission to Stokes emission, which is similar to the study that uses the polarization switching technique [14]. Since the polarization-modulated pulse used in this study can be prepared only by passing a femtosecond pulse through a birefringence crystal, the experimental setup is simple compared to those of other studies [8–11].

This paper is organized as follows. The procedure for the generation of a polarization-modulated pulse by use of a birefringence crystal is discussed in Sec. II. This polarization-modulated pulse is then used in the experiment described in Sec. III. The efficiencies of TSRRS induced by three types of polarization-modulated pulses are discussed in Sec. IV, and then the efficiency is compared to those induced by linearly, circularly, and elliptically polarized pulses. After discussion of the suppression of SPM and the generation mechanism of the rotational anti-Stokes emission, the paper is summarized.
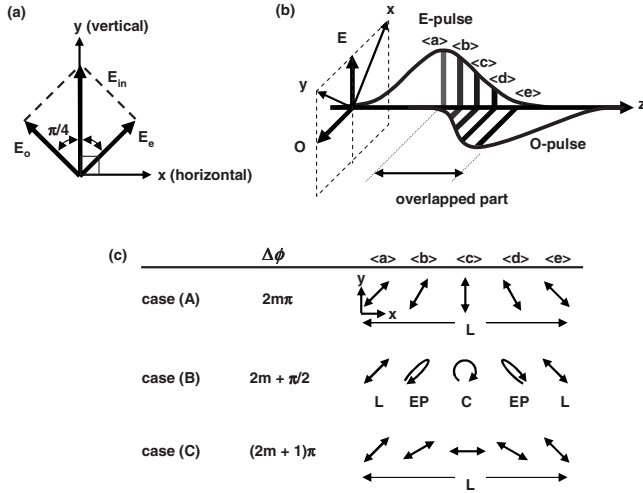
FIG. 1. (a) The relation between the polarization direction of the input beam (y, vertical) and the fast (slow) axis in the LBO crystal. E_{in}, E_o, and E_e show the electric fields of input, ordinary, and extraordinary fields, respectively. (b) Schematic of the shape of the pulse emerging from an LBO crystal. The O pulse and E pulse indicate ordinary and extraordinary pulses, respectively. The polarization of the overlapped part is related to the phase delay between the two pulses and varies rapidly with time as shown in (c), in which the polarization states at $\langle a \rangle$, $\langle b \rangle$, $\langle c \rangle$, $\langle d \rangle$, and $\langle e \rangle$ in (b) are shown for the three cases of the phase delays of $2m\pi$ [case (A)], $(2m+1/2)\pi$ [case (B)], and $(2m+1)\pi$ [case (C)]. L, linear polarization; EP, elliptical polarization; C, circular polarization.

II. THEORY

A. Generation procedure of polarization-modulated pulses

When a vertically polarized femtosecond pulse is passed through a birefringence crystal whose crystal axis is crossed by an angle of $\pi/4$ with the polarization axis of the pulse, the pulse is split into two pulses called ordinary and extraordinary rays (pulses), respectively. As shown in Fig. 1(a), the amplitudes of the ordinary and extraordinary rays are equal to each other, and they propagate with different group velocities. When the two pulses emerge from the crystal, they are separated completely in time from each other provided that the crystal is sufficiently thick. In this case, since the energy of a pulse is divided into two pulses, the peak intensity of the emitting pulse consisting of the ordinary pulse (hereafter denoted by O pulse) and the extraordinary pulse (hereafter denoted by E pulse) is much lower than that of the input pulse. For instance, if the pulse energy of the O pulse is equal to that of the E pulse, the peak intensity of the output pulse is half the intensity of the input pulse. Since a lower intensity pulse leads to a lower efficiency of SPM, the efficiency of SPM induced by the modulated pulse should be lower than the efficiency of SPM induced by a pulse without propagation through the crystal.

Let us then consider the special case in which the thickness of the birefringence crystal is not so thick and the two resulting pulses are partially overlapped by each other. In this case, the polarization of the overlapped part [Fig. 1(b)] depends on the phase delay ($\Delta\phi$) between the ordinary ray and the extraordinary ray, as shown in Fig. 1(c). When the

phase delay is $\Delta\phi = \Delta\phi_A = 2m\pi$ (m is an integer), which corresponds to case (A) shown in the figure, the polarization is linear in all parts of the pulse, though the polarization direction continuously rotates in a clockwise direction with time. At the middle point of the pulse [$\langle c \rangle$ in Fig. 1(b)], where the amplitude of the ordinary pulse is the same as that of the extraordinary pulse, the polarization state is vertical polarization. In the case of $\Delta\phi = \Delta\phi_B = (2m+1/2)\pi$ [case (B) in Fig. 1(c)], the polarization is linear at point $\langle e \rangle$ and varies elliptically with respect to increases in the amplitude of the ordinary ray. At the middle point $\langle c \rangle$, the polarization becomes circular and then varies to elliptical polarization. After that, as shown in the figure, the elliptical polarization changes to linear polarization with a reduction in the amplitude of the ordinary pulse. The directions of the major axes of the two elliptical polarizations [at $\langle b \rangle$ and $\langle d \rangle$ in Fig. 1(b)] are different from each other, and the directions of rotations of the polarizations in all the elliptical and circular polarizations included in the pulse are clockwise. The case of $\Delta\phi_C = (2m+1)\pi$ [case (C) in Fig. 1(c)] is similar to that of case (A), where the polarization is linear in all parts of the pulse, but the direction of the polarization rotates in a counterclockwise direction with time, and the polarization at the middle point [at $\langle c \rangle$ in Fig. 1(b)] is horizontal.

B. Indirect characterization of polarization-modulated pulses

For the characterization of the polarization-modulated pulses, techniques based on spectral interferometry such as polarized light interference versus wavelength of only a glint (POLLIWOG) [15,16] are useful. However, we could not prepare a reference pulse that was completely characterized as required by the interferometric characterization, hence an indirect characterization procedure is discussed here.

We consider a laser pulse with a pulse width of τ_p, a center angular frequency of ω, and a phase $\phi_0(t)$, which is expressed as

$$E(t) = A(t)\exp\{-i[\omega t - \phi_0(t)]\} + \text{c.c.}, \tag{1}$$

where c.c. indicates the complex conjugate and $A(t)$ is the slowly varying envelope (real valued function) of the electric field. If the pulse is passed through a birefringence crystal under the condition discussed above (the angle between the polarization direction of the pulse and the fast axis of the crystal is $\pi/4$ rad), ordinary (E_o) and extraordinary (E_e) pulses emerging from the crystal can be described as

$$E_o(t) = (1/\sqrt{2})A(t)\exp\{-i[\omega t - \phi_0(t)]\} + \text{c.c.},$$

$$E_e(t) = (1/\sqrt{2})\gamma A(t - \Delta\tau)\exp\{-i[\omega t - \phi_0(t) + \Delta\phi]\} + \text{c.c.}, \tag{2}$$

where $\Delta\phi$, $\Delta\tau$, and γ are the phase delay, group delay, and ratio of the amplitude of the extraordinary pulse to that of the ordinary pulse, respectively. The parameter of γ accounts for the energy loss of the extraordinary ray caused by the energy conversion from the ray into its second harmonic, which is the case of the experiment in this study. When Eq. (2) was derived, it was assumed that the group velocity dispersion

induced in the crystal is negligibly small and the two pulses have identical shapes when they leave the crystal; the condition can be realized experimentally by use of a sufficiently thin crystal. If the horizontally polarized field (E_x, x component) and the vertically polarized field (E_y, y component) included in the pulse emerging from the crystal are separated spatially using a polarizer, they can be described as $E_x(t) = -E_o(t)\cos(\pi/4) + E_e(t)\cos(\pi/4)$ and $E_y(t) = E_o(t)\cos(\pi/4) + E_e(t)\cos(\pi/4)$, respectively [see Fig. 1(a)], or, by use of Eq. (2),

$$E_x(t) = R(t)[\gamma A(t - \Delta\tau)\exp(-i\Delta\phi) - A(t)] + \text{c.c.}$$

$$= \widetilde{E}_x(t) + \text{c.c.},$$

$$E_y(t) = R(t)[\gamma A(t - \Delta\tau)\exp(-i\Delta\phi) + A(t)] + \text{c.c.}$$

$$= \widetilde{E}_y(t) + \text{c.c.}, \tag{3}$$

where $R(t)$ is $(1/2)\exp\{-i[\omega t - \phi_0(t)]\}$. The energy ratio ($R_P$) of the horizontally polarized field (P_x) to the vertically polarized field (P_y) is then expressed by

$$R_P = P_x/P_y = \int_{-\infty}^{\infty} |\widetilde{E}_x(t)|^2 dt \bigg/ \int_{-\infty}^{\infty} |\widetilde{E}_y(t)|^2 dt$$

$$= \frac{\int_{-\infty}^{\infty} [(1 + \gamma^2)A(t)^2 - 4\gamma A(t)A(t - \Delta\tau)\cos(\Delta\phi)]dt}{\int_{-\infty}^{\infty} [(1 + \gamma^2)A(t)^2 + 4\gamma A(t)A(t - \Delta\tau)\cos(\Delta\phi)]dt}.$$

$$\tag{4}$$

In deriving the final form in Eq. (4), the time integral of $A(t)^2$ was considered to be equal to that of $A(t - \Delta\tau)^2$. If $A(t)$ is a Gaussian function or sech function, which means $A(t)$ is a positive quantity, the ratio R_P becomes a minimum at $\Delta\phi = \Delta\phi_A = 2m\pi$, unity at the phase delay $\Delta\phi = \Delta\phi_B = (2m + 1/2)\pi$, and a maximum at $\Delta\phi = \Delta\phi_C = (2m+1)\pi$. The above behavior between $\Delta\phi$ and R_P is independent of the value of γ, and the polarizations of the pulses of cases (A), (B), and (C) in Fig. 1(c) can be indirectly characterized by measuring the energy ratio R_P, which is applied in the experiment described below.

C. TSRRS induced by the polarization-modulated pulses

The efficiency of Raman emission in TSRRS depends on the polarization state of the pump pulse. A circularly polarized field leads to the highest gain for the rotational Stokes emission of all polarization states, though no rotational anti-Stokes emission is generated in this case. Both circularly and countercircularly polarized components must be involved in the pump pulse for the generation of a rotational anti-Stokes emission. Though a linearly polarized pulse contains equal amounts of circularly and countercircularly polarized fields, the parametric gain suppression related to Stokes–anti-Stokes coupling [1,17] occurs, precluding rotational Raman emission. Only an elliptically polarized pulse can generate both rotational Stokes and anti-Stokes emissions. The efficiency of the anti-Stokes generation, however, is low com-

pared to that of the Stokes emission in either case of elliptically polarized pulses with small and large ellipticities. In the case of an elliptically polarized pump pulse with small ellipticity, the net amplitude of circular polarization included in the pulse is small, and the amplitudes of coherent rotations and hence rotational anti-Stokes emission are small. In the case of an elliptically polarized pump pulse with large ellipticity, though the net amplitudes of the circular polarization and thus the coherent rotations are large, the amplitude of the countercircular polarization is small and also results in a low efficiency of the anti-Stokes emission.

The pulses of cases (A) and (C) contain only a linearly polarized component, and therefore are expected to result in no Raman emission. When the pulses of cases (A) and (C) are injected into hydrogen gas, they cannot be distinguished from each other, and hence the interactions between the pulses and hydrogen gas, and thus the spectra of the output pulses, would be the same. The pulse of case (B), on the other hand, is completely different from the above cases. At the middle point of the pulse [⟨c⟩ in Fig. 1(b)], the field is circularly polarized, resulting in the generation of Stokes emission and excitation of the coherent rotations of hydrogen molecules through TSRRS. At the same time, the molecules are excited to an upper rotational state, which involves a change in the quantum number M by 2 [18]. With the progress of time, the polarization state of the pump pulse changes from circular to elliptical, and then to linear, which can be considered as an increase in the amount of countercircularly polarized field, and is thus expected to significantly affect the subsequent process of TSRRS. The gain for the Stokes emission should decrease with the progress of time due to the decrease of the net amplitude of the circularly polarized pump field. The circularly polarized rotational anti-Stokes emission, on the other hand, can be generated by interaction between the coherent rotations excited previously and the countercircularly polarized field contained in the pump field, even when the pump field is linearly polarized, although in general TSRRS, which is a linearly polarized pulse, cannot generate rotational Raman emission for the reasons discussed above. Furthermore, it is expected that the ratio of the anti-Stokes emission to Stokes emission is higher than that in the case of an elliptically polarized pump pulse.

III. EXPERIMENT

Experiments in this study were operated using the setup shown in Fig. 2. A femtosecond pulse emitted from a chirped pulse amplifier (CPA; a center wavelength of 784 nm, 1 kHz, a beam diameter of ~6 mm, Concerto, Thales Laser) was used in this study. By passing the pulse (a pulse energy of 740 μJ, a pulse width of 110 fs) through a zero-order half-wave plate (WPQ-7800-2M, Sigma Koki), the polarization of the pulse was changed from horizontal to vertical. The vertically polarized pulse was then passed through a LiB_3O_5 (LBO) crystal (a thickness of 1.58 mm, cutting angles of $\theta = 90°$ and $\phi = 33.2°$, CASTECH) whose fast axis was tilted by $\pi/4$ rad with respect to the polarization direction of the input pulse, as shown in Fig. 1(a). Though several percent of the energy of the near-ir pulse injected into the
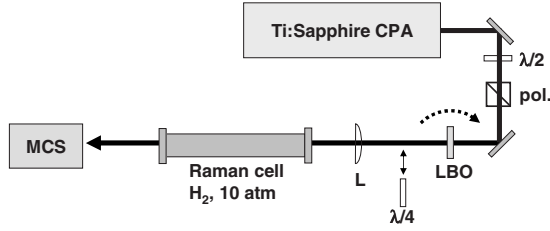
FIG. 2. Experimental setup. $\lambda/2$, half-wave plate; pol., polarizer; LBO, LBO crystal; $\lambda/2$, quarter-wave plate; L, plano-convex lens; MCS, fiber-coupled multichannel spectrometer together with a diffuser.

FIG. 3. The output spectra obtained for the pulses of case A (broken line), B (solid line), and C (dotted line); each spectrum is normalized with respect to its peak intensity. O_{S1}, O_{S2}, and O_{AS1} show the first and second rotational Stokes and the first rotational anti-Stokes emissions of orthohydrogen, respectively. Concerning U (a peak at 838 nm), see text.

crystal was converted to its second harmonic, no care was paid to this harmonic since the small energy loss by the conversion would not be a problem in the indirect characterization of the three types of polarization-modulated pulses discussed above. The output beam from the crystal was then passed through a zero-order quarter-wave plate (WPQ-7800-4M, Sigma Koki) whose fast axis was parallel to the slow axis of the LBO crystal. The pulse was then passed through a polarizer made of calcite to spatially separate the horizontally and vertically polarized components of the beam. After passing the vertically polarized beam through a dichroic mirror to remove the second-harmonic emission, the energy of the pulse was measured with a power meter (PM10,Coherent-Molectron). While monitoring the energy, the incidence angle of the beam entering the LBO crystal was changed by tilting the crystal with respect to the propagation axis of the incident beam. The angle was adjusted to the condition that the energy had a maximum value in order to create a phase delay of $2m\pi$ [$\Delta\phi_A$, case (A)] between the ordinary and extraordinary rays after the quarter-wave plate. If it was necessary, rotation of the quarter-wave plate by $\pi/2$ made the slow axis of the wave plate parallel to the slow axis of the LBO crystal, thereby changing the phase delay to $\Delta\phi_C=(2m+1)\pi$ [case (C)]. The pulse in case (B), which is the case of the phase delay of $\Delta\phi_B=(2m+1/2)\pi$, was also generated by simply removing the quarter-wave plate from the setup.

A polarization-modulated pulse generated using this procedure was then focused into a Raman cell (800-mm-long, 5-mm-thick windows at both ends) filled with pressurized hydrogen gas (10 atm) using a plano-convex lens (fused silica; a focal length, $f=500$ mm). The maximum gas pressure achievable in the Raman cell was 10 atm, and the efficiency in the Raman emissions was the highest at this pressure. The gas pressure in the Raman cell was, therefore, kept at 10 atm in all the experiments described in this paper. The output beam from the Raman cell was recollimated with a plano-convex lens ($f=500$ mm) and was scattered using a diffuser. The diffused light was introduced into a multichannel spectrometer (wavelength resolution of 2.5 nm, spectral range of 300–1100 nm, USB2000, Ocean Optics) through an optical fiber (QP400-2-UV-VIS, Ocean Optics) for the measurement of the time-averaged spectrum of the pulse. Note that the wavelength dependence of the sensitivity of the spectrometer was not calibrated by use of a standard lamp, such as a halogen lamp. The relative intensities of high-order
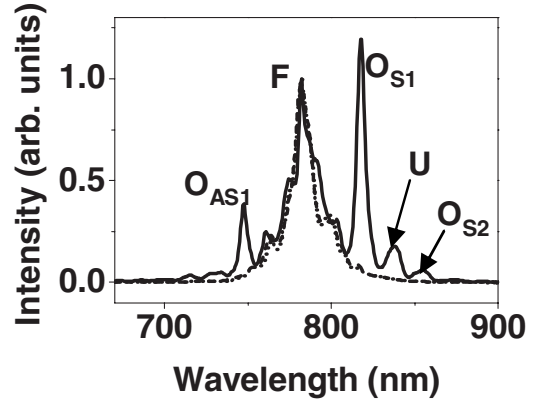
Raman emissions are not discussed in the following description since their frequencies are far from the frequency of the fundamental emission (784 nm) and are not so reliable. Only the relative intensities of the first Raman emissions are discussed.

IV. RESULTS AND DISCUSSION

The spectra of the output pulses from the Raman cell are shown in Fig. 3. As mentioned previously, the spectra of the output pulses obtained in cases (A) and (B) are almost identical, where no rotational Raman lines are generated but the spectral width of the fundamental emission is expanded by the generation of SPM. In case (B), on the other hand, several Raman emissions are observed at 672, 686, 698, 715, 730, 748, 818, 838, 855, 874, and 890 nm. The intensities of the high-order Raman emissions at 672, 686, 715, 874, and 890 nm are weak compared to the low-order Raman emissions generated at the wavelengths of 748, 818, 838, and 855 nm, which are depicted by O_{AS1}, O_{S1}, U, and O_{S2} in Fig. 3, respectively. The frequency shift from the peak wavelength of the fundamental (input) emission (784 nm) to the wavelength of an anti-Stokes line (748 nm) is nearly equal to 587 cm^{-1}, the rotational Raman shift of orthohydrogen. The emission lines in the longer wavelength regions, on the other hand, cannot be easily characterized by the rotational Raman shift of orthohydrogen (587 cm^{-1}) or parahydrogen (354 cm^{-1}). This would be due to modulation of the Stokes frequencies to higher frequencies by the simultaneous generation of SPM [19]. We have found that frequency separation between the wavelengths 784 and 818 nm is 530 cm^{-1}, which corresponds to the separation between 818 and 855 nm. Hence, the two peaks (818 and 855 nm) correspond to the first and second rotational Stokes emissions of orthohydrogen, respectively. Though the peak at 838 nm (U in Fig. 3) could not be characterized, the frequency shift from the spectral component at 802 nm (edge of the fundamental emission) is 530 cm^{-1}, and thus it might be related to the

Stokes emission of orthohydrogen. Though both the rotational Stokes and anti-Stokes emissions were efficiently generated, the ratio of the amplitudes of the anti-Stokes to Stokes emissions was not so large. This might be attributed to the fact that the amplitude of the countercircularly polarized component generating the anti-Stokes emission, which was included in the linearly polarized component [$\langle a \rangle$ in Fig. 1(b)], is smaller than that of the amplitude of the circularly polarized component [$\langle c \rangle$ in Fig. 1(b)] generating the Stokes emission (cf. Sec. II C). The peaks generated at 672, 686, 698, 715, and 730 are not easily characterized. The frequency shift between 748 and 730 nm and the shift between 715 and 698 nm are nearly equal to the Raman shift of parahydrogen. In contrast, the frequency shift between 748 and 715 nm, the shift between 715 and 686 nm, and that between 698 and 672 nm are nearly equal to the Raman shift of orthohydrogen. The conservation law of angular momenta, which must be satisfied for the generation of the anti-Stokes emissions, may be satisfied as the result of the modulation of the polarization state of the anti-Stokes emissions by SPM or cross-phase modulation. The spectral structure at the shoulder of the fundamental emission at 784 nm is slightly complicated. Small peaks are observed at 803 and 761 nm. The frequency separations between these peaks and the fundamental wavelength of 784 nm are slightly smaller than the Raman shift of parahydrogen (354 cm^{-1}). Hence, these peaks would be generated as the result of simultaneous generation of TSRRS, four-wave mixing, and SPM, which modulates the frequency of the Raman emissions of parahydrogen [19].

It is also possible to produce a variety of polarization-modulated pulses by changing the incidence angle of the beam into the crystal and by changing the relation between the direction of the polarization of the input beam and the optical axis of the crystal. The angle of the LBO crystal was changed to increase the ratio of the amplitudes of rotational anti-Stokes to Stokes emissions. The spectrum of the output beam from the Raman cell obtained in this case is shown in Fig. 4(a). The input pulse energy into the hydrogen gas, which was measured just before the focusing lens, was also varied from 0.20 to 0.49 mJ by use of a zero-order half-wave plate and a polarizer placed just before the LBO crystal. This arrangement would have not changed the other experimental condition, except only to afford a slight change in the energy of the extraordinary ray, thus resulting in an insignificant change in the efficiency of the TSRRS. The first rotational Stokes (822 nm) and anti-Stokes (745 nm) emissions of orthohydrogen were generated at input energies of 0.40 and 0.49 mJ. The wavelength 745 nm differed from the predicted wavelength for the first anti-Stokes emission of orthohydrogen, 750 nm. The difference was not due to the influence of SPM, since the wavelength of the first-Stokes emission (822 nm) was not modulated by SPM. The anti-Stokes emission would be generated as the result of the energy conversion from the frequency component at 779 nm, which was separated by 587 cm^{-1} from 745 nm. The efficiency in energy conversion from the fundamental emission to the Raman emissions was increased with increases in the input energy. Up to 13% of the pulse energy was converted to the anti-Stokes emission at the input energy of 0.49 mJ. The
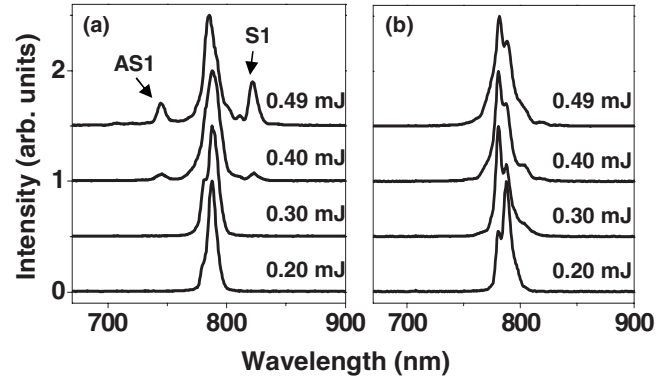
FIG. 4. Output spectra of TSRRS induced by the pulses modulated in the LBO crystal (a) and by the pulses without the modulation (b). The energy of the input pulses before the focusing lens was varied among 0.20, 0.30, 0.40, and 0.49 mJ. S1 and AS1 show the first rotational Stokes emission and the first rotational anti-Stokes emission, respectively. Each spectrum is normalized with respect to its peak intensity.

ratio of the amplitudes of anti-Stokes to Stokes emissions is high compared to the above experiment, especially in the case of an input energy of 0.40 mJ, where the peak heights of the two sidebands are comparable to each other and the peak ratio is 0.9. This cannot be observed in the usual case of SRRS. Small peaks were also generated at 708 and 811 nm in the spectrum when the input energy was 0.49 mJ. The frequency separation between 811 and 788 nm, which is the wavelength of the shoulder of the fundamental emission, is 354 cm^{-1} and corresponds to the Raman shift of parahydrogen. The emission at 708 nm, however, is not easily identified. The separation between 708 and 745 nm is 700 cm^{-1} and much larger than the Raman shifts of orthohydrogen (587 cm^{-1}) and parahydrogen (354 cm^{-1}). One possibility of the origin of the generation of the emission at 708 nm is nonresonant degenerate four-wave mixing among the emissions at 786, 745, and 708 nm since the frequency separation between 786 and 745 nm is also 700 cm^{-1}. Another possible explanation is that a frequency component at 739 nm, which is the shoulder of the strong emission at 745 nm, was shifted by 587 cm^{-1} to generate the emission at 708 nm. For this mechanism, however, the polarization of the component at 739 nm should be circular with the opposite direction to that of the component at 745 nm for the satisfaction of the conservation of angular momenta. Generation of such an anti-Stokes emission with frequency-dependent polarization would be realized as the result of the generation process of the polarization-modulated pulse used in this study. The phase difference between the ordinary and extraordinary rays, emerging from a birefringence crystal used to generate a polarization-modulated pulse, depends on the wavelength of the rays, and thus the polarization state at the center part of the polarization-modulated pulse [$\langle c \rangle$ in Fig. 1(b)] also depends on the wavelength and would lead to such a complicated generation mechanism to generate the emission at 708 nm. The frequency dependence of the polarization within a polarization-modulated pulse should be controlled for understanding completely the generation mechanism of the high-order Raman emissions.
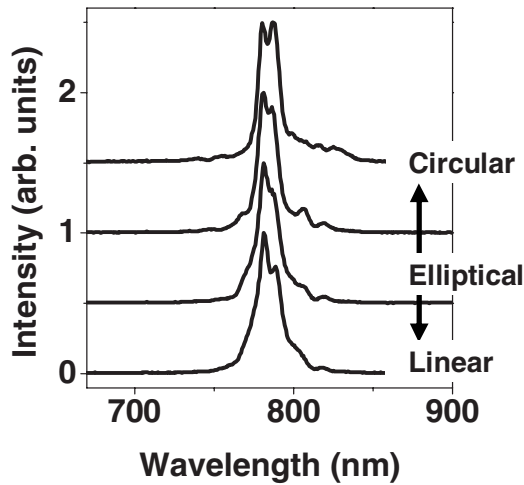
FIG. 5. Output spectra of TSRRS induced by pulses with linear, elliptical, and circular polarizations. The energies of the input pulses are kept at 0.49 mJ. Each spectrum is normalized with respect to its peak intensity.

The low efficiency of SPM is another concern in this experiment. To compare the efficiency in this regime to that in the case of a linearly polarized pump pulse, the LBO crystal was removed from the experimental setup to change the polarization of the input pulse to linear. The output spectra from the gas are shown in Fig. 4(b) for the input energies ranging from 0.20 to 0.49 mJ. The efficiency of SPM was high compared to the case of the result of Fig. 4(a). The spectral width of the fundamental emission is expanded especially for the large energy of the input pulse; the full width at half-maximum (FWHM) of the emission is 13 nm at the input-pulse energy of 0.20 mJ, and is 17 nm at 0.49 mJ. On the other hand, in the case of 0.49 mJ in Fig. 4(a), the spectral width of the fundamental emission is 13 nm, suggesting that the generation of SPM is substantially suppressed in the case of the polarization-modulated pulse compared to the case of a pulse without modulation of polarization. This can be explained by the decrease of the pulse peak intensity caused by the pulse splitting process in the LBO crystal discussed in Sec. II. In the spectra shown in Fig. 4(b), almost no appreciable Raman emission was generated as predicted from the theory of parametric Stokes–anti-Stokes coupling [1,17]. However, a very small peak was observed at 818 nm when the input energy was 0.49 mJ. This might be generated as the result of generation of the seed emission for TSRRS through SPM for subsequent amplification of the emission.

In the general case, TSRRS is induced by a circularly or elliptically polarized pulse, and therefore the result should also be compared to those induced by pulses with such polarizations. In Fig. 5, the output spectra obtained in the case of input pulses with polarizations of a variety of ellipticities are shown. The polarization of an input pulse was controlled using a quarter-wave plate (WPQ-7800-4M, Sigma Koki) and the input energy was kept at 0.49 mJ. None of the output spectra include appreciable peaks related to TSRRS, but instead they do have a unique structure in the wavelength region longer than 800 nm especially in the case of the circularly polarized pulse, which would be caused by the

simultaneous generation of TSRRS and SPM. The efficiency of spectral broadening in the longer wavelength region was varied with the change of polarization, and was most efficient for the circularly polarized input pulse. This is attributed to the fact that the efficiency of the rotational Stokes emission is the highest for circular polarization [20]. The small peaks generated at 805, 818, and 748 nm in the case of the elliptically polarized pulses correspond to the first Stokes emission of parahydrogen, the first Stokes emission of orthohydrogen, and the first anti-Stokes emission of orthohydrogen, respectively, though the wavelengths were slightly shifted by simultaneous generation of SPM [19].

The efficiency of SPM was the lowest in the case of circular polarization, which is suggested from the fact that the spectral width of the fundamental emission is the smallest (15 nm) of all the polarizations. The efficiency of SPM in the case of circular polarization is higher than that in the case of the polarization-modulated pulse [13 nm at 0.49 mJ in Fig. 4(a)]. The efficiency of TSRRS, which is suggested from the peak height of the Stokes emission, is also lower than the result obtained for the polarization-modulated pulse. In other words, the efficiencies of SPM and TSRRS induced by a polarization-modulated pulse are, respectively, lower and higher than those induced by linearly, elliptically, and circularly polarized pulses. This is considered to be attributed to the low intensity of the polarization-modulated pulse, which leads to the low efficiency of SPM and thus a high efficiency of TSRRS, compared to the three types of pulses.

A pulse with a more complex polarization change than those used in this study can be produced using a polarization shaping technique based on a spatial phase modulator [21], which modulates ellipticity as well as the orientation of the elliptical principal axis within a pulse. The technique has already been applied in the study of single-pulse coherent anti-Stokes Raman scattering (CARS), though the ellipticity of the pulse has not been modulated [22]. Since this technique allows one to control the polarization of each spectral component as well as to produce a pulse with arbitral polarization change, various investigations about TSRRS are possible. For instance, one may obtain a higher efficiency of the Raman emissions than this study by locking the phase delay $\Delta\phi$ over all the frequency components included in the pulse, and may control the peak ratio of rotational anti-Stokes to Stokes emissions freely.

The polarization-modulated pulse may be used to solve the problem of the reduced efficiency of the multicolor rotational emissions in the femtosecond regime [6]. If the emission efficiency is improved and multicolor emissions are generated, the emissions can be used to generate ultrashort pulses [23]. Furthermore, it is also interesting to use the polarization-modulated pulse as a pump pulse to generate the coherent rotations of hydrogen molecules for subsequent modulation of the frequency of a uv pulse [11], since the pulse is expected to excite efficiently the coherent rotations without the significant influence of SPM.

V. CONCLUSION

In conclusion, TSRRS induced by a polarization-modulated femtosecond pulse is reported. The ultrafast varia-

tion of polarization within a pulse, created by passing the pulse through a birefringence crystal, generates TSRRS with an efficiency that is much higher than those of TSRRS induced by linearly, elliptically, and circularly polarized femtosecond pulses. The high efficiency is related to the low efficiency of SPM due to the low peak intensity of the pulse compared to a pulse without polarization modulation. Furthermore, the pulse has a unique feature in that rotational Stokes and anti-Stokes emissions are simultaneously generated with high efficiencies, which is explained by the temporal evolution of the ratio of the amplitudes of countercircularly polarized to circularly polarized fields involved in the pulse. Since the polarization-modulated pulse can be generated only by inserting a birefringence crystal into the optical path, it provides a simple system to convert the wavelength of a femtosecond pulse to shorter and longer wavelengths.

[1] Y. R. Shen and N. Bloembergen, Phys. Rev. **137**, A1787 (1965).

[2] N. Bloembergen, Am. J. Phys. **35**, 989 (1967).

[3] T. Imasaka, S. Kawasaki, and N. Ishibashi, Appl. Phys. B: Photophys. Laser Chem. **49**, 389 (1989); L. L. Losev, Y. Yoshimura, H. Otsuka, Y. Hirakawa, and T. Imasaka, Rev. Sci. Instrum. **73**, 2200 (2002); D. D. Yavuz, D. R. Walker, G. Y. Yin, and S. E. Harris, Opt. Lett. **27**, 769 (2002); D. D. Yavuz, D. R. Walker, M. Y. Shverdin, G. Y. Yin, and S. E. Harris, Phys. Rev. Lett. **91**, 233602 (2003).

[4] H. Kawano, C. H. Lin, and T. Imasaka, Appl. Phys. B: Lasers Opt. **63**, 121 (1996); V. Morozov, A. Olenin, and V. Tunkin, *ibid.* **67**, 573 (1998).

[5] V. Krylov, A. Rebane, O. Ollikainen, D. Erni, U. Wild, V. Bespalov, and D. Staselko, Opt. Lett. **21**, 381 (1996); V. Krylov, O. Ollikainen, U. P. Wild, A. Rebane, V. G. Bespalov, and D. I. Staselko, J. Opt. Soc. Am. B **15**, 2910 (1998).

[6] H. Kawano, Y. Hirakawa, and T. Imasaka, Appl. Phys. B: Lasers Opt. **65**, 1 (1997).

[7] R. L. Carman, F. Shimizu, C. S. Wang, and N. Bloembergen, Phys. Rev. A **2**, 60 (1970).

[8] E. Sali, P. Kinsler, G. H. C. New, K. J. Mendham, T. Halfmann, J. W. G. Tisch, and J. P. Marangos, Phys. Rev. A **72**, 013813 (2005).

[9] S. Zaitsu, Y. Kida, and T. Imasaka, J. Opt. Soc. Am. B **22**, 2642 (2005).

[10] M. Wittmann, A. Nazarkin, and G. Korn, Opt. Lett. **26**, 298 (2001).

[11] Y. Kida, T. Nagahara, S. Zaitsu, M. Matsuse, and T. Imasaka, Opt. Express **14**, 3083 (2006).

[12] Y. X. Yan, E. B. Gamble, and K. Nelson, J. Chem. Phys. **83**, 5391 (1985).

[13] J. A. Giordmaine and W. Kaiser, Phys. Rev. **144**, 676 (1966).

[14] K. Midorikawa, H. Tashiro, K. Nagasaka, and S. Namba, Phys. Rev. Lett. **62**, 1263 (1989); Y. Akiyama, K. Midorikawa, M. Obara, and H. Tashiro, Opt. Lett. **16**, 97 (1991).

[15] W. J. Walecki, D. N. Fittinghoff, A. L. Smirl, and R. Trebino, Opt. Lett. **22**, 81 (1997).

[16] A. Smirl, in *Frequency-Resolved Optical Gating: The Measurement of Ultrashort Laser Pulses*, edited by R. Trebino (Kluwer, Boston, 2002), p. 375.

[17] M. D. Duncan, R. Mahon, J. Reintjes, and L. L. Tankersley, Opt. Lett. **11**, 803 (1986); K. Leung, M. Oron, D. Klimek, R. Holmes, and A. Flusberg, *ibid.* **13**, 33 (1988); R. Holmes and A. Flusberg, Phys. Rev. A **37**, 1588 (1988).

[18] R. W. Minck, E. E. Hagenlocker, and W. G. Rado, Phys. Rev. Lett. **17**, 229 (1966).

[19] W. Zinth and W. Kaiser, Opt. Commun. **32**, 507 (1980).

[20] G. V. Venkin, Yu A. Il'inskii, and G. M. Mikheev, Sov. J. Quantum Electron. **15**, 395 (1985).

[21] T. Brixner and G. Gerber, Opt. Lett. **26**, 557 (2001); M. Plewicki, F. Weise, S. M. Weber, and A. Lindinger, Appl. Opt. **45**, 8354 (2006).

[22] D. Oron, N. Dudovich, and Y. Silberberg, Phys. Rev. Lett. **90**, 213902 (2003).

[23] S. Yoshikawa and T. Imasaka, Opt. Commun. **96**, 94 (1993).